Available online at www.sciencedirect.com
ScienceDirect
Earth and Planetary Science Letters 261 (2007) 9–19
EPSL
www.elsevier.com/locate/epsl

High sensitivity mapping of Ti distributions in Hadean zircons

T. Mark Harrison *, Axel K. Schmitt

Department of Earth and Space Sciences and Institute of Geophysics and Planetary Physics, UCLA, Los Angeles, CA 90095, USA

Received 16 February 2007; received in revised form 4 May 2007; accepted 7 May 2007
Available online 13 May 2007
Editor: R.W. Carlson

Abstract

Detrital zircons as old as nearly 4.4 Ga from the Jack Hills, Western Australia, offer possible insights into a phase of Earth history for which there exists no known rock record. Ti concentrations of Hadean zircons indicate a spectrum of crystallization temperatures that range from a cluster at ca. 680 °C to apparent values exceeding 1200 °C. The low temperature peak has been interpreted to indicate the existence of 'wet' melting conditions during the Hadean, but alternate views have been advanced. We have developed methods for quantitative ion imaging of titanium in zircons using positive and negative secondary ions, produced respectively under bombardment of O^- and Cs^+, that permit detailed insights regarding Ti concentration distributions. Each approach has particular advantages that tradeoff in terms of sensitivity, ultimate lateral resolution, and reproducibility. Coupled with high resolution spot analyses, these ion images show that Ti contents greater than about 20 ppm in the Jack Hills zircons are associated with cracks or other crystal imperfections and that virtually all of the high apparent temperatures (i.e., >800 °C) yet obtained are suspect for contamination by Ti extraneous to the zircon. Removing these from consideration strengthens the previous conclusion that the Hadean Jack Hills population is dominated by zircons crystallized at 680–720 °C.

Keywords: zircon; Ti thermometer; ion imaging; Jack Hills

1. Introduction

Due to their inherent resistance to alteration by weathering, dissolution, shock, and diffusive exchange, and their enrichment in U and Th relative to daughter product Pb, zircon is widely recognized as the premiere U–Pb geochronometer (Hanchar and Hoskin, 2003; Cherniak and Watson, 2003). While highly valued in that role, the trace element and isotopic chemistry of zircon is also increasingly recognized as a valuable probe of environmental conditions that existed during crystallization (Hoskin and Schaltegger, 2003). Even in cases where zircon has been removed from its original rock context, such as detrital grains in clastic rocks, trace elements, isotopic signatures, and mineral inclusions can yield important information regarding source conditions [e.g., (Watson and Harrison, 2005; Maas et al., 1992; Harrison et al., 2005)], provided that the record has been faithfully preserved.

Using the Ti concentration in zircon as a crystallization thermometer, Watson and Harrison (Watson and Harrison, 2005, 2006) reported 136 ion microprobe Ti measurements on zircons ranging in age from 3.91–4.35 Ga. The vast majority of Hadean zircons plot in a normal distribution at an average model temperature of 683 ± 27 °C, with a scattered tail defined by apparent

* Corresponding author. Tel.: +1 310 825 7970; fax: +1 310 206 3051.
E-mail address: tmh@oro.ess.ucla.edu (T.M. Harrison).

0012-821X/$ - see front matter © 2007 Published by Elsevier B.V.
doi:10.1016/j.epsl.2007.05.016

values up to ~1200 °C. A similar cluster is also present in 36>4 Ga zircons reported by Valley et al. (2006). This temperature spectrum was interpreted by Watson and Harrison (2005, 2006) as indicating that the Hadean zircons were dominantly sourced from wet, minimum melts under prograde conditions. Others subsequently argued that the low temperature Hadean peak could reflect derivation from zircons that formed during cooling of mafic (Valley et al., 2006; Coogan and Hinton, 2006) or intermediate (Nutman, 2006; Glikson, 2006) magmas.

Conclusions regarding provenance that can be derived from individual detrital zircons depend upon the preservation of their original chemical signatures. For example, Hoskin (2005) concluded that some Jack Hills zircons have undergone hydrothermal alteration that has modified their original composition. However, in the absence of recrystallization or complete loss of crystalline integrity, the extremely low diffusivity of Ti in zircon (Cherniak and Watson, 2006) assures that the distributions imposed during crystallization will be retained indefinitely under virtually all crustal conditions.

Cathodoluminescence (CL) and other electron-based imaging of zircon carried out in conjunction with ion microprobe U–Pb dating has proved very useful in improving the accuracy of the age interpretation (see examples in (Hanchar and Hoskin, 2003)). While valuable for revealing precursor grain nuclei (i.e., restitic cores) and/or compositional zoning and other growth features in zircons, CL imaging is incapable of revealing coherent thermochemical domains (i.e., crystal chemistry associated with growth during a specific thermal history episode) or identifying nanoscale Ti-rich inclusions. Without additional information, the structures typically observed in CL imaging could represent time gaps ranging from hours to hundreds of millions of years. However, complementing CL imaging with ion imaging of Ti in zircon has the potential to identify chemical-isotopic regions associated with discrete crystallization events. This approach can furthermore identify anomalously high Ti values due to sub-micron Ti-rich phases that could otherwise be incorrectly interpreted in terms of anomalously high temperatures.

In this paper, we develop techniques for ion imaging Ti distributions in zircon and apply both these methods and spot analysis to >4 Ga zircons from Jack Hills, Western Australia. We find that grains yielding high (>800 °C) apparent crystallization temperatures from conventional spot analyses are contaminated by elevated amounts of Ti contained along cracks. Furthermore, high resolution imaging of Ti within Hadean zircons tends to reveal a narrow temperature range of crystallization temperatures in individual grains. While as yet a limited data set, these data are more consistent with zircon forming in low temperature partial melts relative to crystallization during cooling mafic or intermediate magmas.

2. Analytical details

The high-spatial resolution ion microprobe is the preferred tool to measure low levels of Ti in zircon. Titanium concentrations of ca.1–10 ppm (Watson and Harrison, 2005, 2006) in most Hadean Jack Hills zircons are below the detection limit of the electron microprobe and close to that of laser ablation ICPMS analysis. However, at low mass resolution using an O^- primary beam, doubly-charged ions of ^{92}Zr, ^{94}Zr and ^{96}Zr interfere with singly-charged ions of ^{46}Ti (8.25%), ^{47}Ti (7.44%) and ^{48}Ti (73.72%), respectively. To avoid these interferences, Watson and Harrison (2005) determined Ti concentration in zircons by analyzing the low abundance isotope $^{49}Ti^+$ (5.41%) using a CAMECA *ims*3f. Without exploiting the highest abundance isotope, ^{48}Ti, high resolution ion imaging of Ti distributions is not feasible for the low Ti concentrations that characterize many zircons. Operated at high mass resolving power (MRP), the CAMECA *ims*1270 permits the major Ti secondary ion species, $^{48}Ti^+$, to be resolved from $^{96}Zr^{2+}$. However, analysis at high mass resolving power sacrifices intensity and thus the full 14-fold higher abundance of ^{48}Ti relative to ^{49}Ti will not be realized in increased sensitivity.

For samples with heterogeneous Ti concentrations, ion imaging offers the best prospect for understanding the source of the variations (i.e., geologically significant or due to inclusions or other localized features). However, charge build-up due to removal of the conducting Au coating during O^- bombardment can impact the focusing of the primary beam and alter secondary ion yields as a function of pit geometry. An alternative approach is to measure negatively charged Ti secondary ion species (e.g., TiO^-) produced by Cs^+ bombardment in conjunction with charge compensation provided by a low energy, normal incidence, electron flood gun. This approach has the advantage that doubly-charged negative secondary ions are unknown (i.e., no isobaric interferences from ZrO^{2-} species) thus permitting low resolution/high sensitivity analysis. Moreover, a Cs^+ primary beam can be readily focused to very small (~1 μm) spots to enhance spatial resolution. The principal disadvantage of using a Cs^+ primary beam is the lower useful ion yield of any negatively charged Ti ion species compared to Ti^+. An evaluation of the tradeoffs associated with these approaches to ion imaging Ti distributions in zircon is described below.

2.1. Positive secondary ions

Spot analyses were made using a primary O^- beam of ~5 nA focused to a ~20 μm spot. An MRP of ~8500 (10% valley definition) was used to separate $^{48}Ti^+$ from $^{96}Zr^{2+}$ resulting in a decrease of ion transmission to about 60%. Under minimum required MRP conditions, we determined useful yields of ^{48}Ti and ^{49}Ti of 53 and 6.6 cps/ppm Ti/nA, respectively. Thus high MRP analysis of ^{48}Ti yields an 8-fold increase in effective sensitivity relative to ^{49}Ti (at MRP=3500). Note that an MRP of 8500 does not completely resolve $^{48}Ca^+$ (0.187% Ca) from $^{48}Ti^+$, but the contribution of the $^{48}Ca^+$peak on NIST 610 glass, which contains 12% CaO (or ~150 ppm ^{48}Ca), amounts to <1% of the $^{48}Ti^+$ peak. However, $^{48}Ca^+$ is a possible interference when a calcium-rich phase (e.g., apatite, plagioclase) is encountered in the ion beam. Given that mass scans of the unknowns showed little if any contribution from this interference, we decreased MRP to ~7000 for ion imaging in order to enhance transmission. In any case, we note that calcium was not observed in cracks at levels above the detection limit of energy dispersive X-ray analysis (~1%) and thus $^{48}Ca^+$ interferences would contribute <20 ppm apparent Ti in the ion images. Given that cracks are invariably associated with far higher Ti contents, we conclude that any such effect has negligible influence on our interpretations.

Epoxy mounts containing the zircons were polished to 1 μm diamond paste, ultrasonically cleaned in a sequence of soapy water, deionized water, and a 1M HCl solution, and then Au coated. Isotope ratios were measured using a multi-collector, with $^{48}Ti^+$ collected in the axial ETP electron multiplier and $^{30}SiO^+$ measured with a Hamamatsu Mk-3 electron multiplier on the low mass side. To monitor inter-element fractionation and relative multiplier gain, we measured SL13 (15.3% Si, 6.32±0.17 ppm Ti; (Aikman, 2007)) and 91500 zircon (15.3% Si, ca. 5.4–5.8 ppm Ti) over the course of the analyses. We also periodically measured NIST610 glass (32.7% Si, 434±7 ppm Ti; (Pearce et al., 1997)) to assess reproducibility. Spot analyses of ^{48}Ti using NIST610 glass and SL13 zircon were found to be typically reproducible to ±0.7% and ±4%, respectively (see Supplementary Data). Replicate spot analyses performed with synthetic, nominally Ti-free, zircon (0–Ti) yielded a mean Ti concentration of 0.24±0.04 ppm which we regard as our detection threshold. Following spot analysis, samples were lightly re-polished, cleaned, and Au coated for ion imaging measurements.

For ion imaging, we used a 50 pA primary O^- beam focused to a 3–5 μm spot rastered at 20 kHz over a 75×75 μm region. The area overlapping the spot analyses is pre-rastered for ~5 min using a ~1 nA O^- primary beam. A dynamic transfer deflection synchronizes the primary beam raster with secondary ion beam deflection such that the secondary beam was constantly aligned with the center of the field aperture. Although ion yields vary greatly across the rastered field due to charging, this effect can be compensated for by ratioing the Ti data to simultaneously measured $^{30}SiO^+$, which is homogeneously distributed throughout zircon. Integration times were varied as a function of Ti concentrations and ranged between 100 and 500 cycles (1 cycle=15 s).

2.2. Negative secondary ions

Secondary ion intensities for $^{48}Ti^-$, $^{48}TiO^-$, and $^{48}TiO^{2-}$determined for Cs^+ bombardment of rutile scaled as 1:350:100, and consequently we elected to analyze the most abundant species, $^{48}TiO^-$, for which there is no significant doubly charged interference. The useful yield of $^{48}TiO^-$ of 12.3 cps/ppm Ti/nA Cs^+ is about four times lower than that obtained for $^{48}Ti^+$. Our ability to control sample charging with the normal incidence electron flood gun does not appear to significantly improve the determination of Ti concentrations relative to our approach with O^- primary ions. However, the potential to focus the Cs^+ beam to a spot ~4 times smaller than O^-at the same primary intensity (~50 pA) means that we are able to achieve appreciably higher spatial resolution.

For tests undertaken with the Cs^+ beam, mount FC27 was re-polished, cleaned and Au-coated as described above. Following ~5 min of pre-sputtering with a ~200 pA primary beam, a ~50 pA primary beam was rastered over a 25×25 μm area. We found rastering of areas exceeding 50×50 μm not useful because of charging and concomitant intensity loss at the edges due to deflection of the low energy electron beam away from the primary beam spot. For each image, $^{30}SiO_2^-$ and $^{48}TiO^-$ were collected using electron multipliers in multi-collection mode over a total integration time of ~15 min.

2.3. Image processing and quantification

All image files containing raw intensities in 256×256 pixels were imported into the image processing program ENVI©. A low band pass filter was applied, averaging 3×3 pixels (below the spatial resolution of the beam) for each mass to reduce the number of zero or undefined pixel values resulting from zero counts in either numerator or denominator mass. Titanium counts ($^{48}Ti^+$ and $^{48}TiO^-$, for positive and negative secondary ion analysis, respectively) were then normalized to counts of a silicon species ($^{30}SiO^+$ and $^{30}SiO_2^-$, respectively).

Our initial experiments utilized two synthetic zircons (courtesy of E.B. Watson), assumed to be homogeneous, one containing 25±2 ppm Ti (Hi–Ti) and the other notionally Ti-free (0–Ti). Ion images of both $^{48}Ti^+$ (Fig. 1A) and $^{30}SiO^+$ (Fig. 1B) from Hi–Ti show significant spatial variability in ion intensity due to charging effects across the Au-free rastered region, particularly in the center of the field (also note edge effects). Fig. 1C and D demonstrate the effect of the low pass filter (3×3 pixels) that increases the value density without compromising spatial resolution. Assuming that the decreased transmission at higher ion energies affects both species equally, variations in $^{48}Ti^+/^{30}SiO^+$ can be interpreted in terms of heterogeneously distributed Ti. As expected, this plot (Fig. 1E) shows a uniform distribution of Ti supporting this assumption. Note that the variability of region of interest (ROI) $^{48}Ti^+/^{30}SiO^+$ ratios is ~10%, similar to the variability of the spot analyses (Fig. 1F), and that, compared to the average of $^{48}Ti^+/^{30}SiO^+$ in spot analysis mode (0.25±0.02), $^{48}Ti^+/^{30}SiO^+$ measured over nine ROI is on average 50% higher (0.37±0.04). We attribute this difference in secondary ion yield to the systematic suppression of molecular $^{30}SiO^+$ relative to $^{48}Ti^+$ within the rastered area due to offset energy distributions. An imaging mode $^{48}Ti^+/^{30}SiO^+$ relative sensitivity factor (RSF) of 0.6 was obtained, or 1.5 times the spot analysis RSF of 0.4. The empirical sensitivity increase for $^{48}Ti^+$ relative to $^{30}SiO^+$ on the high-Ti image (Fig. 1F) was used to calculate Ti concentration from measured $^{48}Ti^+/^{30}SiO^+$. Ti abundances from individual spot analyses agree within uncertainty with the corresponding regions in the Ti concentration maps, thus providing an independent check on the accuracy of the quantification and the effect of mass interferences (e.g., ^{48}Ca). We are currently exploring ion imaging of correlated contaminating species (e.g., Al, Ca, Fe, REE, Pb) in mono-collection and multi-collection modes.

3. Prior Ti analysis of Jack Hills zircons

Zircons from the Narryer Gneiss Complex of Western Australia, including the Jack Hills (Compston and Pidgeon, 1986), yield ages as old as nearly 4.4 Ga (Compston and Pidgeon, 1986; Harrison et al., 2005). As the only known remnants of the Hadean Eon, >4 Ga zircons currently represent our best opportunity to gather chemical information regarding the history of differentiation and crust formation on early Earth. Their very existence extends the history of crust formation to ~400 Ma earlier than that represented by the oldest known rock (Bowring and Williams, 1999). The elevated (relative to mantle values) oxygen isotopic signature preserved in some of these zircons suggests that their host granites were derived from partial melting or assimilation of sedimentary rocks, which in turn implies a Hadean hydrosphere (Cavosie et al., 2005; Mojzsis et al., 2001; Nemchin et al., 2006; Trail et al., in press). Harrison et al. (2005) measured initial $^{176}Hf/^{177}Hf$ ratios in a suite of 4.01–4.37 Ga zircons from Jack Hills revealing large ε_{Hf} deviations from bulk Earth, consistent with the view that continental crust had formed by ~4.5 Ga.

The vast majority of the Hadean zircons from Jack Hills thus far analyzed for Ti yield concentrations between 1–10 ppm (Watson and Harrison, 2005, 2006; Valley et al., 2006). In the original studies of Watson and Harrison (2005, 2006), care was taken to avoid inclusions of Ti-rich minerals and other crystal imperfections (e.g., cracks). Nevertheless, a single, unseen rutile inclusion of 100-nm-diameter in a 10-μm-diameter analysis spot would increase apparent temperature from 700 to

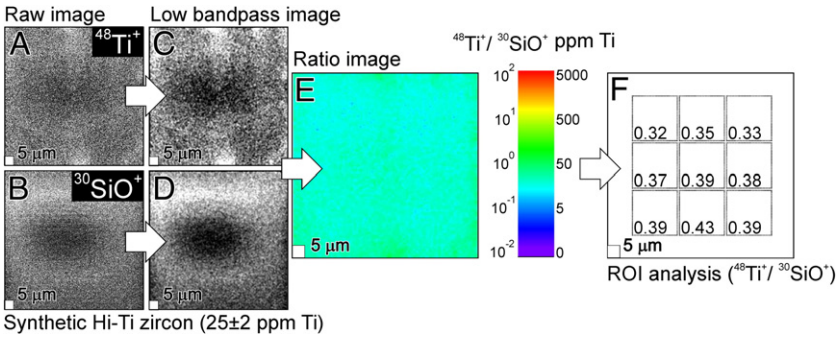

Fig. 1. Flow-chart illustrating ion image processing and quantification. Synthetic Hi–Ti zircon (25 ppm Ti) is used as an example. 256×256 pixel raw images (A, B) for each mass ($^{48}Ti^+$ and $^{30}SiO^+$) are generated by adding counts from all cycles (white: high intensity). Each pixel value is then replaced by the average of neighboring pixels in a 3×3 square to reduce the number of zero value pixels (low bandpass image; C, D). Pixels are ratioed, and a color scale is applied (for better comparison, we used the same color scale in this Fig. and Fig. 3). $^{48}Ti^+/^{30}SiO^+$ ratios are computed over regions of interest (ROI; F). Ti concentrations are calculated from $^{48}Ti^+/^{30}SiO^+$ using an empirical relative sensitivity factor of 0.6 (see text).

>1000 °C. Because a nominally 10-μm-diameter primary ion beam includes a diffuse halo that extends beyond the apparent crater region, analyses close to cracks containing very high Ti could also yield anomalously high temperatures.

Assuming a_{TiO2} and a_{SiO2} activities of unity, model temperatures for Hadean zircons define a broad range with a dominant peak in the probability distribution at 683±27 °C (Watson and Harrison, 2005, 2006). For Hadean zircons of magmatic origin, it would be a rare case in which formation occurred where a_{TiO2} and a_{SiO2} were ≤0.6. Since similar sub-unity values of a_{TiO2} and a_{SiO2} are essentially compensatory (Ferry and Watson, in press), a calculated temperature of ~680 °C would only be underestimated by between 0 and 40 °C.

4. Results

We report 158 Ti concentration measurements on 34 Jack Hills zircons ranging in age from 4.11 to 4.38 Ga (Fig. 2A; Table 1 in Appendix). Calculated temperatures using the calibration of Watson and Harrison (2005) range from 590–1380 °C (assuming $a_{TiO2}=a_{SiO2}=1$). On the basis of these analyses, we selected seven zircons for further characterization by Ti ion imaging as being representative of different emergent patterns. For example, apparent temperatures for FC27 3–11 are highly variable, including extreme (>1300 °C) values, and the spatial pattern appears discordant to growth zones indicated by CL imagery. In contrast, ANU125 15–5 yields low and relatively uniform Ti contents. Fig. 3A–G shows a sequence of images for each grain; from left to right they are the backscattered electron image, the CL image, and the Ti ion image overlain on the secondary electron image. Spot analysis locations are also shown on the latter image. In contrast to Watson and Harrison (2005, 2006), we aimed to densely space multiple analysis spots on individual grains, largely disregarding potential crystal imperfections such as cracks that might otherwise have been avoided.

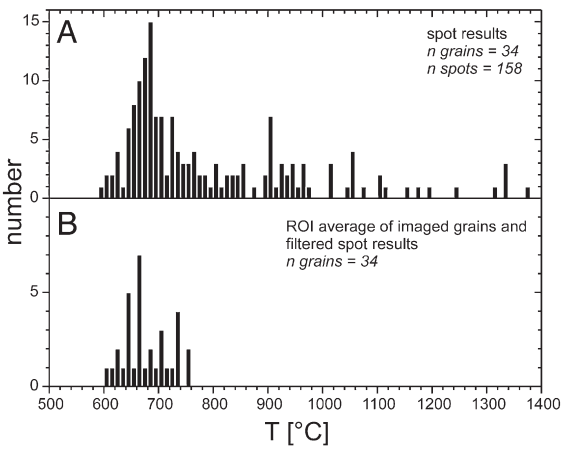

Fig. 2. Histogram of 158 Ti concentration measurements on 34 Jack Hills zircons (A) and the interpreted temperature from combined ion imaging and spot analyses (B).

In each of the figures we have plotted a square corresponding to the size of the O^- beam used in acquiring the rastered images to emphasize that the apparent lateral extent of Ti concentration anomalies is limited by this scale. For example, a 100-nm-inclusion of a Ti-rich mineral will appear as a ca. 5 μm sized 'hot spot'.

4.1. FC27 3–11

Electron imaging of this zircon suggests a core-rim relationship with abundant lateral and radial fractures in the higher U rim. Energy dispersive X-ray analyses of these features show no signal from calcium, thus restricting the contribution from a ^{48}Ca interference on ^{48}Ti to a trivial level. Multiple U–Pb analyses (Fig. 4A) of this grain are consistent with formation of the core domain at 4.38 Ga with the overgrowth developing at ca. 4.1 Ga. Variable amounts of Pb* loss result in a broad distribution of apparent ages. Spot Ti concentrations vary from 25 ppm in the core to 706 ppm in the rim region. Ion imaging, however, indicates that the minimum temperature in the rim region is 685 °C and that a broad region in the core has uniform Ti (13±2 ppm) that we interpret as corresponding to the crystallization temperature of the core (i.e., 730±12 °C). The boundaries between the core and rim and cracks across the rim are all characterized by high, and locally very high (>1000 ppm) Ti contents. A small region with extremely high Ti concentrations (>2000 ppm) to the upper right of the Fe-oxide inclusion (Fig. 3A) consists of zircon decomposition products. Electron beam X-ray analysis demonstrated that this enrichment is associated with decomposed zircon (i.e., domains mainly consisting of microcrystalline mixtures of ZrO_2 and SiO_2).

It is possible that some of this Ti contamination was introduced during sample preparation. Evidence of this effect is suggested by an experiment in which we juxtaposed crystal faces of synthetic zircons Hi–Ti and 0–Ti and sectioned the couple in an epoxy mount. While ion imaging revealed that portions of this artificial boundary were essentially Ti-free, irregularly-spaced Ti 'hot spots' were also observed indicating that Ti was introduced during sample preparation. However, where cracks or other boundaries reveal high and relatively uniform Ti abundances, we infer this to be intrinsic to the sample.

As noted earlier, the spatial resolution of these images is limited by the ca. 4 μm O^-spot and thus it is unclear from the images obtained under O^- bombardment whether the high Ti zones are entirely restricted to cracks or if they penetrate diffusely into the zircon. To assess this possibility, we re-imaged FC27 3–11 using a 1 μm Cs^+ beam and imaged in TiO^-. As seen in Fig. 4, the apparent size of the Ti-rich zones decreases proportionality to the smaller size of the rastering beam. We thus conclude that the contaminating Ti is restricted to within 1 μm of cracks and other crystal imperfections.

4.2. ANU125 1–13

Electron images show typically igneous growth zoning with the suggestion of an unconformity (Fig. 3b). The $^{207}Pb/^{206}Pb$ age of this grain is 4118±

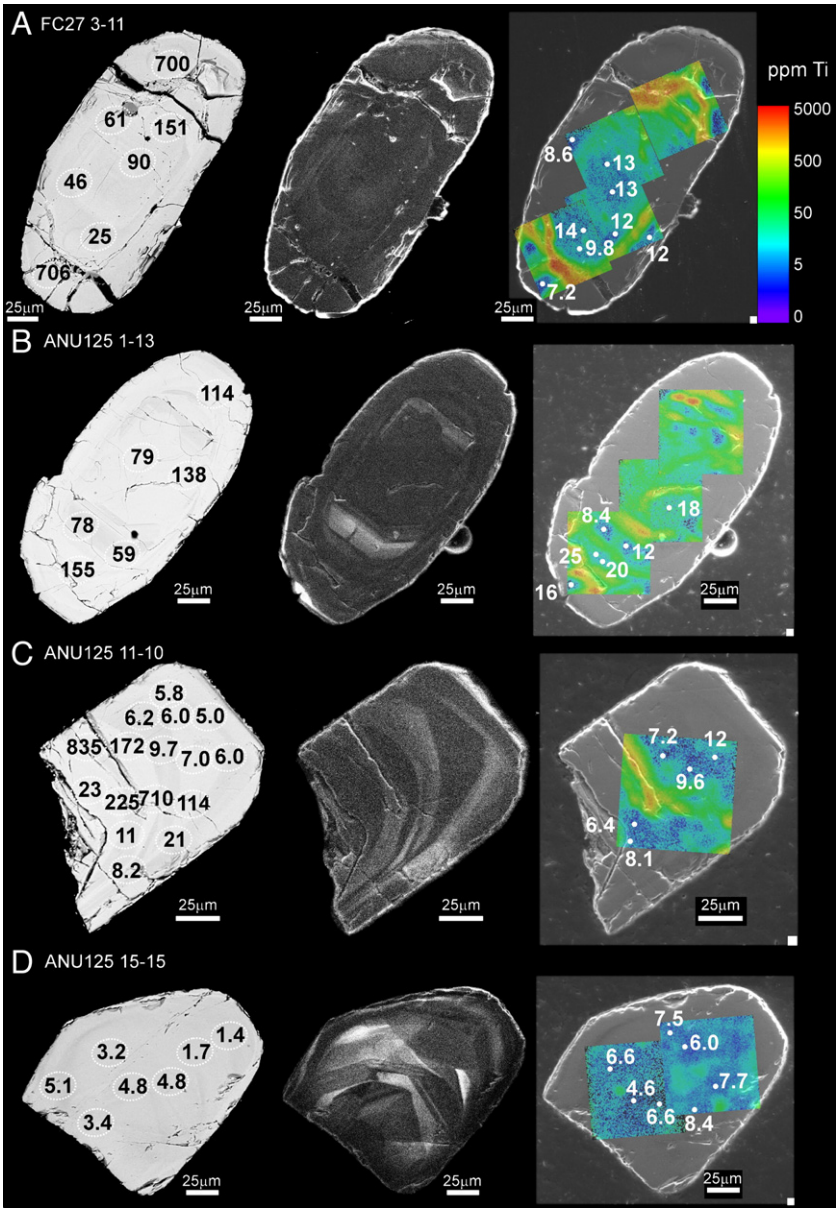

Fig. 3. Each of the figure sequences from A) to G) shows the back scattered electron image, the cathodoluminescense (CL) image and the Ti ion image overlain on the secondary electron image. A) FC27 3–11; B) ANU125 1–13; C) ANU125 11–10, D) ANU125 15–15; E) ANU52 7–12; F) ANU63 3–14, G) ANU64 8–9. Arrow in A) points to Fe-oxide inclusion. Note that color scale is the same as in Fig. 1.

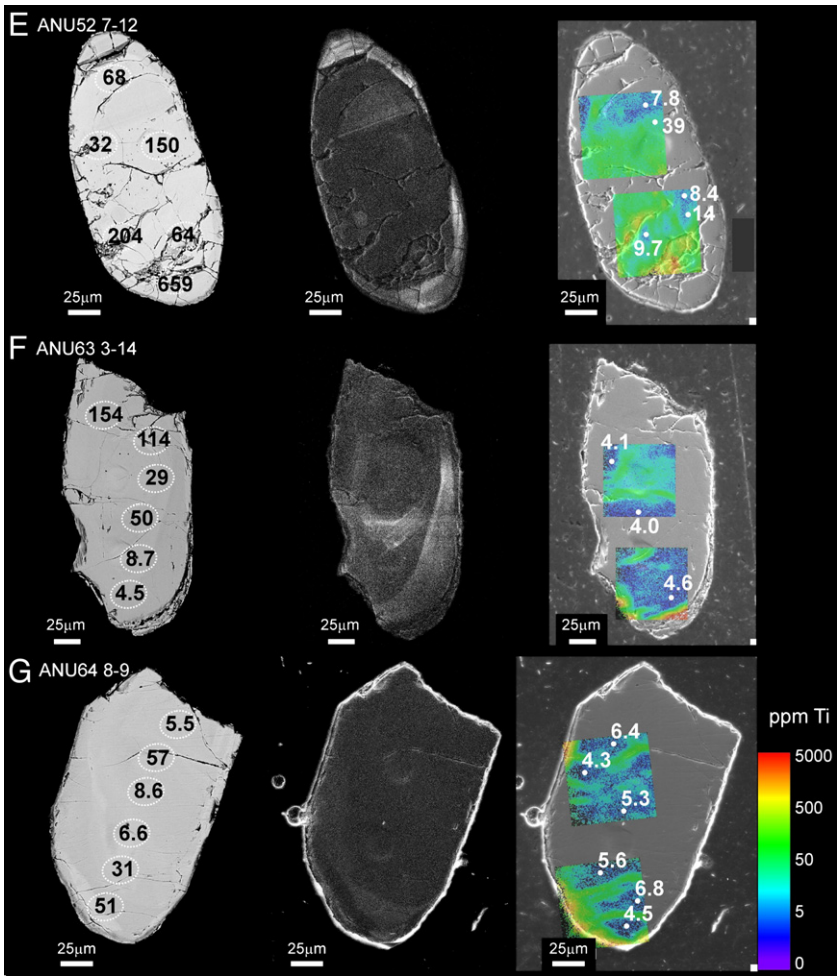

Fig. 3 (*continued*).

5 Ma (12% discordant). The range of Ti contents obtained by spot analysis (155–59 ppm) corresponds to a temperature interval of 1050 °C to 925 °C and thus could conceivably reflect growth during magma cooling from high temperature. However, the pattern of calculated temperatures does not have a simple relationship to the growth zones observed in CL. Furthermore, ion imaging again shows that the high spot concentrations correspond to zones of high Ti which correlate to cracks, both at growth interfaces and at acute angles to them. From ion imaging, we infer that core and rim Ti concentrations away from cracks are essentially indistinguishable, (~17 ppm) and correspond to a crystallization temperature of ~750 °C. An intermediate ~20 μm wide CL-bright oscillatory band yields slightly lower temperatures (~710 °C), suggestive of a minor transient decline in magmatic temperature during crystallization.

4.3. ANU125 11–10

This zircon fragment, with a $^{207}Pb/^{206}Pb$ age of 4143 ± 9 Ma (1% discordant), shows patterns in BSE and CL indicative of igneous zoning (Fig. 3C). The principal feature of the ion image is a band of high (>1000 ppm) Ti concentration along a large crack system that cuts across the pattern of growth zoning. Spot values were measured as high as 835 ppm adjacent to the crack. In contrast, the 6 analyses closest to the top of the grain are restricted to the range 5 to 7 ppm. In the absence of any obvious contaminating hot spot, we interpret this to indicate a model temperature for this portion of the crystal of 690 ± 15 °C. Ion imaging shows an essentially homogeneous temperature distribution with an average of 698 ± 20 °C (average Ti = 8.7 ± 2.3 ppm), in good agreement with the result from the uncontaminated spot analyses near the top of the grain. Despite complex CL-banding, Ti thermometry

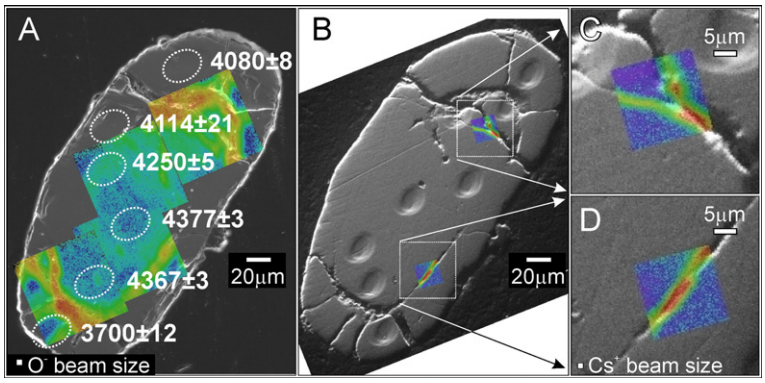

Fig. 4. Secondary electron images of FC27 3–11 with Ti ion image overlays produced by (A) positive ion analysis using a ~4 μm O^- primary beam and (B) negative ion analysis with a ~1 μm Cs^+ primary beam. Enlargements of the negative ion Ti maps are displayed in C) and D). Ion microprobe $^{207}Pb/^{206}Pb$ ages for FC27 3–11 are shown in A). Note that sputter pits in B) are unrelated to Ti and U–Pb age analysis, and were produced by Cs^+ bombardment for oxygen isotopic analysis.

reveals that the entire grain originally formed as a single thermochemical domain.

4.4. ANU125 15–15

CL imaging of this zircon fragment, with a $^{207}Pb/^{206}Pb$ age of 4115 ± 16 Ma (3% discordant), shows clear evidence of igneous growth zoning (Fig. 3D). The crystal contains fewer large cracks relative to those already discussed and shows only minor Ti concentration anomalies in the ion image. Spot analyses reveal a relatively low dispersion in Ti (5.1 to 1.4 ppm). Nonetheless, minor anomalies in the ion image suggest that the highest values (4.8–5.1 ppm) reflect minor Ti contamination. The Ti-image shows small (less than the beam diameter) 'hot spots' in which Ti concentrations are up to 10-times elevated. These spots are irregularly distributed on the surface, and uncorrelated to CL patterns. We suspect that they may represent surficial Ti contamination, albeit much less severe than extrinsic Ti associated with cracks and zircon decomposition products (see above). Note that any surface contamination will have stronger effects on the ion image because of the slower sputter rate resulting from the ~100 times less intense primary beam current and rastering over a larger area compared to spot analysis mode.

Temperatures calculated from the Ti ion images avoiding these 'hot spot' regions (679 ± 15 °C) agree well with the core temperatures from the spot analyses. The spot results are consistent with formation of the core at 655 °C followed by cooling to a temperature of 600 °C during crystallization of the rim. If these temperatures are accurate, this distribution is seen as more consistent with formation following anatexis rather than retrograde crystallization from high (>800 °C) temperature [see (Harrison et al., in press)].

4.5. ANU52 7–12

The core of this grain (Fig. 3E) yields a $^{207}Pb/^{206}Pb$ age of 4253 ± 3 Ma (8% discordant). It appears to be rimmed by later zircon growth with CL structure of a type associated with precipitation under either igneous or metamorphic conditions. The grain is substantially cracked and appears to contain anastomosing regions of high Ti content clearly visible in the Ti ion image. We suspect that essentially all Ti spot analyses are affected by contamination. In the upper Ti image, we find a sharp temperature contrast between 840 °C and 691 °C (39 and 7.8 ppm Ti, respectively) that corresponds to a transition from dark CL in the core to an adjacent intermediate bright-CL domain. While this high-Ti core may represent high temperature zircon growth, we find much lower temperatures around 700 °C in other uncontaminated regions within the same CL-dark core. The high-Ti domains may thus alternatively represent a heavily damaged zone that is affected by secondary Ti-uptake.

4.6. ANU63 3–14

CL imaging of this zircon fragment, with a $^{207}Pb/^{206}Pb$ age of 4267 ± 12 Ma (8% discordant), shows evidence of igneous growth zoning (Fig. 3F). Spot Ti analyses range in concentration from 154 ppm to 4.5 ppm. The lowest spot concentration of 4.5 ppm (675 °C) is from near the rim and appears not to be influenced by Ti introduced along cracks. Ion imaging was directed to two regions of low crack density in the middle and lower portions of the grain. Ti concentrations in regions free from cracks (4.3 ± 0.3 ppm) agree with the lowest spot concentration, and indicate temperature uniformity throughout the grain

(645±5 °C). Notably, zones with variable CL brightness are again indistinguishable in their Ti abundances and temperatures.

A novel feature in our collection of Ti ion images is that grain ANU63 3–14 shows a rim with extremely high (>2000 ppm) Ti concentrations. This high-Ti mantle is not an artifact of the raster area overlapping a grain boundary, because no such feature is present in the ion image on ANU125 15–15 that overlaps a grain boundary and adjacent epoxy mounting medium and potentially represents a coating of secondary origin.

4.7. ANU64 8–9

Unlike essentially all other samples, electron beam imaging of this 4209±3 Ma (3% discordant) zircon fragment does not clearly suggest a formation environment. High Ti contents are associated with several fine cracks and a prominent crack near the upper-right edge of the grain. The two Ti spot analyses obtained away from the fractures of 6.6 and 5.5 ppm are interpreted to reflect the formation temperature of this zircon (i.e., 690–706 °C), but these may represent maximum values due to beam overlap with cracks. Ti ion image analysis yields a slightly lower average temperature of 663±14 °C for the least crack-affected areas on the grain. Again, we note a high-Ti coating on this grain, similar to that on ANU63 3–14.

5. Discussion

It is clear from inspection of the ion images in Fig. 3A–G that Ti concentration distributions in the seven imaged zircons do not generally exhibit patterns expected for zircon growth under either a prograde or retrograde crystallization history (i.e., the patterns tend not to correlate with crystal morphology or CL growth zones). Instead, they reveal Ti 'hot spots' that appear to be associated with cracks. In virtually all cases, spot analysis concentrations are consistent with ion image data given the lateral resolution limitation of ca. 4 μm.

Our ion imaging results showing the distribution of Ti in Hadean zircons have implications for the temperature spectra inferred from conventional spot analyses. Fig. 2A shows apparent temperatures calculated for the 158 spot analyses reported in Table 1 (Appendix). This dataset, which yields an average temperature of 796±172 °C, independently reproduces the salient features of earlier reports (Watson and Harrison, 2005, 2006) of a peak at ~680 °C and scattered values to temperatures greater than 1200 °C. Based on our imaging studies, we surmise that samples yielding highly variable Ti concentrations, including values of >100's of ppm, are contaminated by exogenous Ti.

For the samples on which we carried out Ti ion imaging, we can use ROI analysis to discount data that were influenced by contaminant Ti. With the possible exception of grains ANU125 1–13 and ANU52 7–12, all imaged grains show a restricted range of Ti away from cracks that corresponds to temperature variations of <50 °C. As mentioned earlier, we infer that these zones are actually much narrower than they appear in Fig. 3 due to the ca. 4 μm spot size. While the apparent temperature range recorded in grains ANU125 1–13 and ANU52 7–12 (697–792 °C and 691–840 °C, respectively) could represent a real indication of zircon crystallization over an extended temperature interval, clear core to rim temperature zonations are absent and secondary Ti contamination cannot be ruled out. In any case, the remarkable temperature uniformity of most zircons studied here suggests relatively simple crystallization histories that belie possible impressions fostered by complex internal CL structures developed within these regions. In fact, we find that CL pattern complexity may misleadingly invite speculation about polyphase zircon growth histories that are unsupported by Ti-in-zircon thermometry data obtained in ion imaging mode [cf. (Nemchin et al., 2006)].

For spot analyses alone, we apply a simple filter: the lowest Ti concentration is taken to represent an upper bound on the apparent crystallization temperature. While this may have the effect of ignoring actual gradients in temperature resulting from crystallization over a protracted interval [see (Harrison et al., in press)], imaged variations are typically <50 °C [this study, 4] and thus this approach is unlikely to significantly influence our overall conclusion. Fig. 2B summarizes the interpreted temperature distribution of the 34 grains examined in this study. Their average temperature of 678±42 °C is 118 °C lower than that of the raw results. Among the 34 grains studied, temperatures of >750 °C are exceedingly rare (Fig. 2B), compared to eight out of fifteen zircons extracted from modern oceanic gabbros (Coogan and Hinton, 2006).

While others have argued that this distribution could result from zircon growth in cooling mafic and intermediate (Valley et al., 2006; Coogan and Hinton, 2006; Nutman, 2006; Glikson, 2006) magmas, Harrison et al. (in press) showed that the Hadean and mafic zircon temperature distributions are statistically distinct and that zircons from the two environments are characterized by an order of magnitude difference in average U concentration. The only known example of a zircon-bearing extrusive lava from a mid-ocean ridge yields an

average Ti concentration of 14 ppm, corresponding to a model temperature of 771 °C (Perfit et al., 2006). Based on over 300 Ti analyses of Hadean zircons with interpreted temperatures overwhelmingly <750 °C [this study, (Watson and Harrison, 2005, 2006; Valley et al., 2006)], it is highly unlikely that zircon crystallization in basaltic differentiates (Coogan and Hinton, 2006) contributed significantly to the detrital Hadean zircon population from Jack Hills.

Using a data constrained model of zircon growth, Harrison et al. (in press) also showed that intermediate magmas could not be a dominant source of the low temperature Hadean peak. They further noted that preservation effects in detrital populations will tend to reduce the appearance of zircons formed at low temperatures (ca. 700 °C) relative to those formed from either mafic or intermediate melts.

Our ~680 °C average is indistinguishable from that previously inferred from the cluster in the continuous spectrum (Watson and Harrison, 2005, 2006; Harrison et al., in press). The salient feature of this result is the low and restricted range of apparent crystallization temperatures. Even assuming crystallization in the presence of $a_{TiO2}=0.6$, this average only rises to ~720 °C. Thus the simplest explanation for the dominant low temperature Hadean peak continues to be that it reflects prograde partial melting under conditions at or near water saturation. Indeed, our inability in this study to document an actual crystallization temperature in excess of 760 °C opens the real possibility that none of the substantially higher temperature outliers previously reported are accurate.

6. Conclusions

The potential of the Ti-in-zircon thermometer as a probe to identify coherent thermochemical domains is significantly enhanced by utilization of ion imaging. We investigated the use of rastering both O^- and Cs^+ ion beams across extended portions of zircon crystals to reveal complex Ti distributions at lateral resolutions of ~4 and ~1 μm, respectively. In both cases, non-uniform charging across the investigated area can be compensated for by normalization to a SiO species. These applications are illustrated using Hadean zircons that were previously interpreted to have formed dominantly at ca. 680 °C, but with values ranging beyond 1200 °C. Quantitative ion imaging of Ti, coupled with high density spot analyses, show that the Ti contents associated with these very high apparent temperatures were introduced into the crystal along cracks and are thus unrelated to zircon formation. When these spurious temperatures are removed, only a cluster at 678±42 °C remains which is over 100 °C lower than the average of the unfiltered data set. These results bolster the interpretation of Watson and Harrison (2005, 2006) that the Hadean zircons were dominantly sourced largely from 'wet' or near water-saturated minimum melts under prograde conditions.

Acknowledgements

This work was supported by NSF grant EAR-0635969, ARC grant DP0666497, and a grant from the UCRP program of Lawrence Livermore National Laboratory. We acknowledge facility support from the Instrumentation and Facilities Program of the National Science Foundation. We thank Bruce Watson, Kevin McKeegan, and Rick Ryerson for helpful discussions, Bruce again for supplying the synthetic zircons, Janet Harvey and Gilles Peltzer for assistance with image manipulation, Michelle Hopkins for SEM imaging, and Frank Mazdab and Calvin Miller for constructive reviews.

Appendix A. Supplementary data

Supplementary data associated with this article can be found, in the online version, at doi:10.1016/j.epsl.2007.05.016.

References

Aikman, A.B., 2007. Tectonics of the eastern Tethyan Himalaya. Ph.D. thesis. Australian National University.

Bowring, S.A., Williams, I.S., 1999. Priscoan (4.00–4.03 Ga) orthogneisses from northwestern Canada. Contrib. Mineral. Petrol. 134, 3–16.

Cavosie, A.J., Valley, J.W., Wilde, S.A., E.I.M.F., 2005. Magmatic $\delta^{18}O$ in 4400–3900 Ma detrital zircons: a record of the alteration and recycling of crust in the Early Archean. Earth Planet. Sci. Lett. 235, 663–681.

Cherniak, D.J., Watson, E.B., 2003. Diffusion in zircon. Zircon. Revs. Mineral. Geochem., vol. 53, pp. 113–143.

Cherniak, D.J., Watson, E.B., 2006. Ti diffusion in zircon. EOS (Trans., Am. Geophys. Union) 87, V31F–02.

Compston, W., Pidgeon, R.T., 1986. Jack Hills, evidence of more very old detrital zircons in Western Australia. Nature 321, 766–769.

Coogan, L.A., Hinton, R.W., 2006. Do the trace element compositions of detrital zircons require Hadean continental crust? Geology 34, 633–636.

Ferry J.M., and Watson, E.B., in press. New thermodynamic models and revised calibrations for the Ti-in-zircon and Zr-in-rutile thermometers. Contrib. Mineral. Petrol. doi:10.1007/s00410-007-0201-0.

Glikson, A., 2006. Comment on "Zircon thermometer reveals minimum melting conditions on earliest Earth". Science 311, 779a.

Hanchar, J.M., Hoskin, P.W.O. (Eds.), 2003. Zircon. Revs. Mineral. Geochem., vol. 53. 345 pp.

Harrison, T.M., Blichert-Toft, J., Müller, W., Albarède, F., Holden, P., Mojzsis, S.J., 2005. Heterogeneous Hadean hafnium: evidence of continental crust at 4.4 to 4.5 Ga. Science 310, 1947–1950.

Harrison, T.M., Watson, E.B., and Aikman, A.K., in press. Temperature spectra of zircon crystallization in plutonic rocks, Geology.

Hoskin, P.W.O., 2005. Trace-element composition of hydrothermal zircon and the alteration of Hadean zircon from the Jack Hills, Australia. Geochim. Cosmochim. Acta 69, 637–648.

Hoskin, P.W.O., Schaltegger, U., 2003. The composition of zircon and igneous and metamorphic petrogenesis. Rev. Mineral. Geochem. 53, 27–62.

Maas, R., Kinny, P.D, Williams, I.A., Froude, D.O, Compston, W., 1992. The Earth's oldest known crust: a geochronological and geochemical study of 3900–4200 Ma old detrital zircons from Mt. Narryer and Jack Hills, Western Australia. Geochim. Cosmochim. Acta 56, 1281–1300.

Mojzsis, S.J., Harrison, T.M., Pidgeon, R.T., 2001. Oxygen-isotope evidence from ancient zircons for liquid water at the Earth's surface 4300 Myr ago. Nature 409, 178–181.

Nemchin, A.A., Pidgeon, R.T., Whitehouse, M.J., 2006. Re-evaluation of the origin and. Evolution of >4.2 Ga zircons from the Jack Hills metasedimentary rocks. Earth Planet. Sci. Lett. 244, 218–233.

Nutman, A.P., 2006. Comments on "Zircon thermometer reveals minimum melting conditions on earliest Earth". Science 311, 779b.

Pearce, N., Perkins, W., Westgate, J., Gorton, M., Jackson, S., Neal, C., Chenery, S., 1997. A compilation of new and published major and trace element data for NIST SRM 610 and NIST SRM 612 glass reference materials. Geostand. Newsl. 21, 115–144.

Perfit, M.R., Smith, M.C., Schmitt, A.K., Rubin, K.H., 2006. Silicic magma evolution at Mid-Ocean Ridges: insights from the southern Juan de Fuca Ridge, AGU Fall Meeting Abstract V51E–1716.

Trail, D., Mojzsis, S.J., Harrison, T.M., Schmitt, A.K., Watson, E.B., and Young, E.D., in press. Constraints on Hadean zircon protoliths from oxygen isotopes, REEs and Ti-thermometry. Geochem. Geophys. Geosyst. doi:10.1029/2006GC001449.

Valley, J.W, Cavosie, A.J., Fu, B., Peck, W.H., Wilde, S.A., 2006. Comment on "Heterogeneous Hadean Hafnium: Evidence of continental crust at 4.4 to 4.5 Ga". Science 312, 1139a.

Watson, E.B., Harrison, T.M., 2005. Zircon thermometer reveals minimum melting conditions on earliest Earth. Science 308, 841–844.

Watson, E.B., Harrison, T.M., 2006. Response to Comments on "Zircon thermometer reveals minimum melting conditions on earliest Earth". Science 311, 779c.